https://doi.org/10.5194/wes-2026-102
Preprint. Discussion started: 29 June 2026

eawe european academy of wind energy
Open Access WIND ENERGY SCIENCE DISCUSSIONS

Brief communication: Enhanced wind turbine fatigue load estimation using digital shadows with data-driven bias correction

Hadi Hoghooghi and Carlo L. Bottasso
Wind Energy Institute, Technical University of Munich, 85748 Garching b. München, Germany
Correspondence: Carlo L. Bottasso (carlo.bottasso@tum.de)

Abstract. This study proposes a digital shadow framework for wind turbine load estimation that integrates a linearized industrial-grade aeroelastic model with a deep learning–based bias correction (BC) method. To address model mismatches and limited inflow representation, a learning-based bias correction strategy is introduced, where static bias terms are first calibrated via wind-speed-dependent fitting, followed by perturbed correction profiles and parametric simulations to construct a digital shadow dataset. A neural network (NN) is then trained to map operating conditions and bias parameters to load estimation errors, enabling adaptive correction under unseen conditions.

The proposed method is validated using field data spanning diverse inflow conditions, achieving a reduction in blade bending moment DEL prediction errors at the 25% span location from 15–25% to below 5%. This demonstrates strong robustness and improved capture of inflow–structure interactions. Overall, the framework provides a scalable pathway to data-driven digital shadows and a foundation for future digital twin applications in real-time load estimation and operational optimization.

1 Introduction

Digital twins for wind turbine applications have emerged as high-fidelity, data-driven representations of physical assets, playing a key role in next-generation wind energy systems. They enable advanced control via real-time state estimation and feedback optimization (Anand and Bottasso, 2023), support fatigue and remaining useful life prediction through load and degradation modeling (Branlard et al., 2020b; Song et al., 2023), and enhance condition monitoring using anomaly detection and fault diagnosis techniques (Olatunji et al., 2021; Hoghooghi and Bottasso, 2026b). By integrating physics-based aeroelastic models with machine learning algorithms, digital twins allow continuous model updating, parameter identification, and uncertainty quantification under stochastic operating conditions, ultimately improving predictive accuracy and operational performance (Hoghooghi and Bottasso, 2026b, a).

Among the various possible implementations, we follow and extend the digital-shadow framework based on aeroservoelastic models combined with Kalman filtering introduced in Grewal and Andrews (2014); Branlard (2019); Branlard et al. (2024); Hoghooghi et al. (2024); Hoghooghi and Bottasso (2026b). Wind turbine manufacturers already possess trusted and validated aeroservoelastic models, making them strong candidates for filter-internal models. Their use provides immediate predictive capability without requiring extensive field measurements, which are often necessary for purely data-driven approaches. At the

https://doi.org/10.5194/wes-2026-102
Preprint. Discussion started: 29 June 2026

eawe european academy of wind energy
Open Access WIND ENERGY SCIENCE DISCUSSIONS

same time, these physics-based white-box models can be progressively enhanced through data-driven corrections, naturally evolving into adaptive grey-box representations (Hoghooghi and Bottasso, 2026a).

Even when a high-fidelity industrial model is unavailable, a sufficiently representative aeroelastic model—whether open-source or research-oriented—can still be employed as the internal model, while BC terms account for discrepancies between the model and the real turbine (Hoghooghi and Bottasso, 2026b). If no physics-based model is accessible, state-space representations can be identified directly from operational data using system identification techniques such as N4SID (Van Overschee and De Moor, 1996), ERA/OKID (Juang and Pappa, 1985), or ARX/ARMAX formulations (Ljung, 1999). In cases where even this structure is unavailable, fully data-driven estimators such as LSTM or TCN models (Hochreiter and Schmidhuber, 1997; Lea, 2017) can be used to infer loads from SCADA data, although such approaches generally sacrifice physical interpretability and formal model consistency.

This work advances digital twin development by introducing digital shadows derived from high-fidelity multibody dynamics models, linearized for computational efficiency and augmented with flow estimators and data-driven learning components. The proposed framework enables adaptive and accurate representation of wind turbine behavior across a wide range of operating conditions. Building on our previous work (Hoghooghi and Bottasso, 2026b, a), an aeroservoelastic model is linearized around multiple operating points to construct a state-space internal model within a filtering framework. A Kalman filter assimilates SCADA data to update predictions, providing accurate estimates of system states and derived quantities.

This paper presents three key novel contributions.

First, an industrial-grade, encrypted aeroelastic model (Bladed (DNV, 2023)) is employed for linearization, ensuring consistency with industrial workflows. The digital shadow leverages wind-speed-based scheduling inherent to Bladed, enabling realistic operation across the full operational envelope. This situation may represent a scenario in which an original equipment manufacturer (OEM) develops a digital shadow for one of its turbine types, leveraging the aeroelastic model already available during design and/or certification. However, since we can also work with an encrypted model, the situation might also apply to the case of a different party, e.g. a consulting company, that develops an accurate digital shadow, without the need for the OEM that designed that turbine to disclose the large amount of proprietary information that is typically contained in an aeroelastic model.

Second, a data-driven bias correction strategy based on deep learning is introduced to mitigate model-plant mismatch and limitations in scheduling under varying inflow conditions. The correction terms are applied to both the dynamic force balance and output equations, and are learned from data as functions of the operating state. This approach enables nonlinear, state-dependent compensation, improving model fidelity while preserving physical consistency and robustness in fatigue-relevant load estimation.

Third, the framework is validated using field data in simple and complex inflow conditions, including high-shear and non-stationary atmospheric conditions. By learning latent relationships between measurements and unmodeled dynamics, the proposed approach enhances the adaptability of the digital shadow and improves the accuracy of fatigue load predictions under realistic operating conditions.

https://doi.org/10.5194/wes-2026-102
Preprint. Discussion started: 29 June 2026

eawe european academy of wind energy
Open Access WIND ENERGY SCIENCE DISCUSSIONS

Fatigue loads are a key driver of structural degradation in blades, towers, and drivetrains, directly affecting turbine lifetime and operational costs (Hoghooghi et al., 2019, 2020). Improving digital shadow fidelity is therefore essential for proactive maintenance and lifecycle optimization (Hoghooghi et al., 2024). Numerous fatigue estimation approaches exist, including SCADA-based hybrid methods (Noppe et al., 2016), lookup tables (Mendez Reyes et al., 2019), modal expansion (Iliopoulos et al., 2016), ensemble techniques (Abdallah et al., 2017), machine learning and neural networks (Evans et al., 2018; Schröder et al., 2018), polynomial chaos expansion (Dimitrov et al., 2018), deconvolution (Jacquelin et al., 2003), load extrapolation (Ziegler et al., 2017), virtual sensing (Vettori et al., 2020), and NN-based surrogates (Guilloré et al., 2024). This work instead focuses on improving the digital shadow itself via data-driven bias correction to enhance fatigue prediction and condition monitoring accuracy across operating conditions.

The paper is structured as follows. Section 2 presents the methodology, including the internal model, its scheduling, and the proposed adaptive correction strategies. Section 3 evaluates the performance using field data in various inflow conditions, including very challenging ones. Finally, Sect. 4 summarizes the key findings and outlines directions for future work.

2 Methods

The proposed digital shadow framework is illustrated in Fig. 1. A Kalman filter fuses SCADA measurements with a reduced-order model (ROM) obtained from a linearized high-fidelity multibody turbine model. Blade load measurements, together with SCADA signals, are used to estimate inflow conditions in real time, enabling adaptive updates to filter parameters that account for varying operating states and inflow dynamics.

The present formulation builds on the work presented in Hoghooghi and Bottasso (2026b), and uses essentially the same filter-internal model (Sect. 2.1) and observers (Sect. 2.2). To make this article self-contained and improve readability, we have decided to repeat here the presentation of these two elements of the digital shadow, although similar information is also available in our earlier work (Hoghooghi and Bottasso, 2026b).

2.1 Filter-internal model

We employ a nonlinear multibody wind turbine model described by generalized displacements $\boldsymbol{q}$, velocities $\boldsymbol{v}$, and inputs $\boldsymbol{u}$. Noisy measurements $\boldsymbol{\nu}$ correct the outputs $\boldsymbol{y}$ of the filter update, while additional "monitoring" outputs $\boldsymbol{z}$ are estimated but excluded from the innovation step because not associated with corresponding measurements. A ROM is obtained by linearizing the nonlinear system around multiple equilibrium conditions $(\boldsymbol{q}_0, \boldsymbol{v}_0, \boldsymbol{u}_0)$, with corresponding outputs $\boldsymbol{y}_0$ and $\boldsymbol{z}_0$. To account for model mismatch, BC terms are introduced in both the state and output equations. The resulting linearized model, expressed

https://doi.org/10.5194/wes-2026-102
Preprint. Discussion started: 29 June 2026

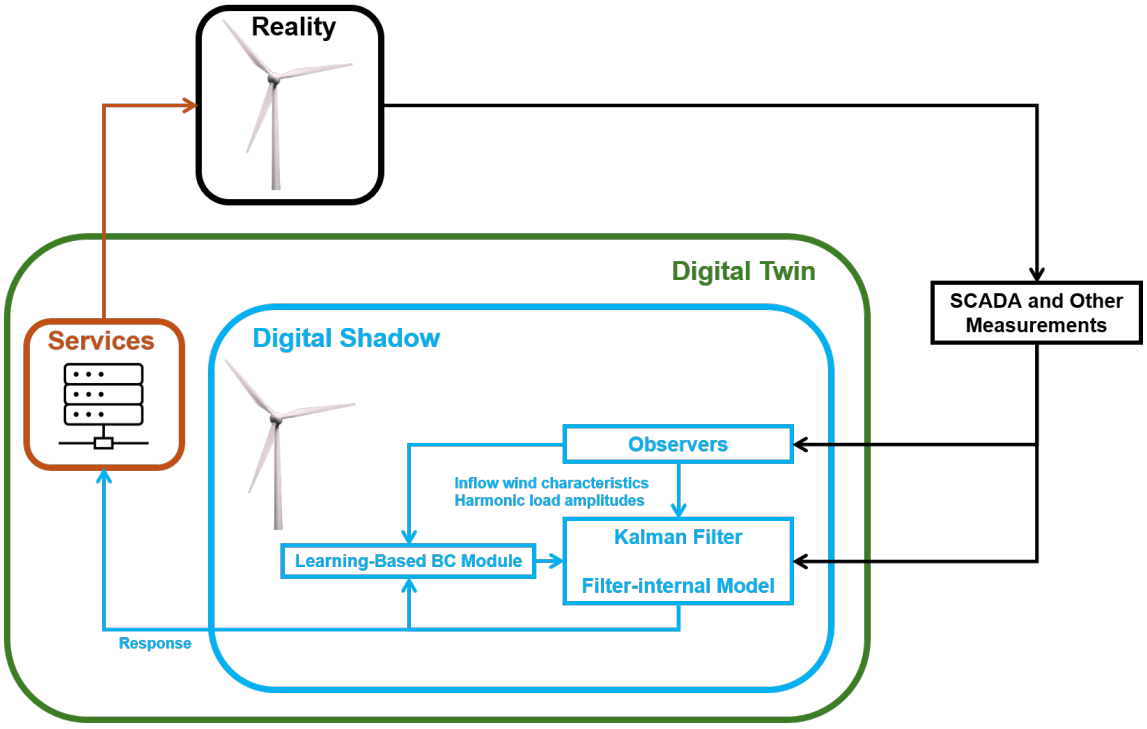

Figure 1. Schematic representation of the proposed digital shadowing framework with learning-based BC.

in terms of increments $\delta(\cdot)$, is:

$$\dot{\delta \boldsymbol{q}} = \delta \boldsymbol{v}, \tag{1a}$$

$$\dot{\delta \boldsymbol{v}} = -\mathbf{M}^{-1}(\mathbf{C}\delta \boldsymbol{v} + \mathbf{K}\delta \boldsymbol{q} + \mathbf{U}\delta \boldsymbol{u} + \boldsymbol{f}_0 + \boldsymbol{\omega}), \tag{1b}$$

$$\dot{\boldsymbol{b}} = \boldsymbol{\omega}_b, \tag{1c}$$

$$\delta \boldsymbol{y} = \mathbf{D}_v \delta \boldsymbol{v} + \mathbf{D}_q \delta \boldsymbol{q} + \mathbf{E}\delta \boldsymbol{u} + \boldsymbol{b} + \boldsymbol{\nu}, \tag{1d}$$

$$\delta \boldsymbol{z} = \mathbf{F}_v \delta \boldsymbol{v} + \mathbf{F}_q \delta \boldsymbol{q} + \mathbf{G}\delta \boldsymbol{u}, \tag{1e}$$

where $\mathbf{M}$, $\mathbf{C}$, $\mathbf{K}$, and $\mathbf{U}$ denote the mass, damping, stiffness, and control matrices, respectively. All noise terms are assumed zero-mean and uncorrelated (Grewal and Andrews, 2008). The correction term $\boldsymbol{f}_0$ compensates for steady-state model mismatch by introducing additive forces in the dynamic equilibrium, generating corrected static deflections as a function of the operating condition through the scheduling parameters $\boldsymbol{s}$. A second correction is introduced through the output bias term $\boldsymbol{b}$ in Eq. (1d), accounting for measurement and sensor biases. Following standard Kalman filtering practice (Grewal and Andrews, 2008), $\boldsymbol{b}$ is modeled as an additional state following a random walk driven by process noise $\boldsymbol{\omega}_b$.

The filter-internal model includes 9 DOFs, with generalized displacements defined as

$$\boldsymbol{q} = \left\{ d_T^{FA}, d_T^{SS}, \psi, d_{B1}^F, d_{B2}^F, d_{B3}^F, d_{B1}^E, d_{B2}^E, d_{B3}^E \right\}^T, \tag{2}$$

https://doi.org/10.5194/wes-2026-102
Preprint. Discussion started: 29 June 2026

eawe european academy of wind energy
Open Access WIND ENERGY SCIENCE DISCUSSIONS

where d_T^{FA} and d_T^{SS} denote the tower fore-aft (FA) and side-side (SS) deflections, ψ is the rotor azimuth, and d_{Bi}^F and d_{Bi}^E are the flapwise and edgewise deflections of blade i. The associated velocities are given by $\boldsymbol{v} = \dot{\boldsymbol{q}}$.

The input vector contains both ambient inflow and control variables:

$$\boldsymbol{u} = \{V, \alpha, k_h, \theta_{\text{coll}}, Q_{\text{gen}}\}^T, \tag{3}$$

where V is the wind speed, α the vertical shear exponent, k_h the horizontal shear, θ_{coll} the collective pitch angle demand, and Q_{gen} the collective generator torque demand. Rotor-equivalent wind speed is estimated from the power coefficient (Hoghooghi and Bottasso, 2026b), while vertical and horizontal shears are obtained using the rotor-as-a-sensor approach (Bertelè et al., 2024).

The measured output vector contains 9 components:

$$\boldsymbol{y} = \left\{\ddot{d}_T^{FA}, \ddot{d}_T^{SS}, \dot{\psi}, m_{B1}^F, m_{B2}^F, m_{B3}^F, m_{B1}^E, m_{B2}^E, m_{B3}^E\right\}^T, \tag{4}$$

where $\ddot{d}_T^{FA}$ and $\ddot{d}_T^{SS}$ are the tower-top accelerations, $\dot{\psi}$ is the rotor speed, and m_{Bi}^F and m_{Bi}^E denote the flapwise and edgewise blade-root bending moments.

The model is scheduled using the parameter vector $\boldsymbol{s}$. This means that linearizations are performed about equilibrium conditions $\boldsymbol{q}_0(\boldsymbol{s})$, $\boldsymbol{v}_0(\boldsymbol{s})$, and $\boldsymbol{u}_0(\boldsymbol{s})$ that depend on $\boldsymbol{s}$; as a consequence all system matrices also depend on the same scheduling parameter, i.e. $\mathbf{M}(\boldsymbol{s})$, $\mathbf{C}(\boldsymbol{s})$, $\mathbf{K}(\boldsymbol{s})$, and $\mathbf{U}(\boldsymbol{s})$. Linearizations are performed at discrete operating points, and the corresponding matrices and equilibrium values are stored in lookup tables (LUTs). During runtime, the current operating condition is estimated online, and interpolation is used to recover the appropriate system matrices and map filter-predicted increments back to nonlinear physical quantities.

2.2 Observers

In this work, the scheduling parameter includes only the rotor-equivalent wind speed V, i.e., $\boldsymbol{s} = \{V\}$. In reality, in general equilibrium points and the corresponding linearized system matrices depend also on other conditions, such as the horizontal and vertical shears and the yaw misalignment angle, as in fact used in Hoghooghi and Bottasso (2026b). The decision to schedule only by wind speed is driven by the fact that the aeroelastic model implemented in Bladed does not support linearizations that depend on these additional parameters (DNV, 2023).

Although not included in the scheduling parameters, vertical and horizontal shears are estimated as described below, and affect the digital shadow response through the input vector $\boldsymbol{u}$ (see Eq. 3).

In the current implementation, the observer outputs are sequentially provided as inputs to the Kalman filter. Although these variables could alternatively be included directly in an augmented filter formulation, the sequential approach is adopted here for simplicity and to leverage previously validated observer implementations (Hoghooghi et al., 2024; Hoghooghi and Bottasso, 2026b, a).

https://doi.org/10.5194/wes-2026-102
Preprint. Discussion started: 29 June 2026

eawe european academy of wind energy
Open Access WIND ENERGY SCIENCE DISCUSSIONS

2.2.1 Wind speed observer

The rotor-equivalent wind speed is estimated by inverting the power coefficient relation:

$$C_p(\theta_{\text{coll}}, \lambda) = \frac{Q_{\text{aero}}\Omega}{0.5\rho A V^3}, \tag{5}$$

where $\lambda = \Omega R/V$ is the tip-speed ratio, R is the rotor radius, $A = \pi R^2$ the swept area, Q_{aero} the aerodynamic torque, and ρ the air density. This relation is stored as a lookup table (LUT), yielding:

$$V = \text{LUT}_{C_p}(\theta_{\text{coll}}, \Omega, Q_{\text{aero}}, \rho/\rho_{\text{ref}}). \tag{6}$$

At runtime, the measured collective pitch θ_{coll} and rotor speed Ω are combined with the estimated aerodynamic torque, approximated as $Q_{\text{aero}} \approx Q_{\text{gen}} + J\dot{\Omega}$, where J is the rotor inertia. Air density is obtained from temperature using the gas law. This LUT-based inversion of precomputed C_p maps is widely used for wind speed estimation in turbine control (Soltani et al., 2013; Bottasso et al., 2018; Schreiber et al., 2020). Noise amplification from differentiating Ω is reduced through filtering and the smoothing effect of LUT interpolation.

2.2.2 Shear and misalignment observers

Vertical shear, horizontal shear, and yaw misalignment are estimated using the rotor-as-a-sensor concept (Kim et al., 2023; Bertelè et al., 2024), which infers inflow characteristics from their signatures in turbine load responses. The estimation is based on harmonic load amplitudes and is expressed as

$$c_E = NN(\boldsymbol{p}, \boldsymbol{i}_M), \tag{7}$$

where c_E represents the estimated quantity (vertical shear α, horizontal shear k_h, or yaw misalignment γ), and $NN(\cdot,\cdot)$ is a single-output neural network with parameters $\boldsymbol{p}$. Separate networks are trained for each variable.

The input vector is defined as

$$\boldsymbol{i}_M = \{\boldsymbol{m}^T, V, \rho\}^T, \tag{8}$$

where $\boldsymbol{m}$ contains the harmonic load amplitudes:

$$\boldsymbol{m} = \{m_{1c}^{OP}, m_{1s}^{OP}, m_{1c}^{IP}, m_{1s}^{IP}\}^T. \tag{9}$$

Here, $(\cdot)_{1c}$ and $(\cdot)_{1s}$ denote the 1P cosine and sine components, while $(\cdot)^{OP}$ and $(\cdot)^{IP}$ indicate out-of-plane and in-plane directions. These quantities are obtained from measured flapwise and edgewise blade loads, transformed into the rotor-disk reference frame using the current blade pitch angle.

The wind speed and shear observers adopted here were previously developed and experimentally validated for the turbines considered in this study (Schreiber et al., 2020; Bertelè et al., 2021).

https://doi.org/10.5194/wes-2026-102
Preprint. Discussion started: 29 June 2026

eawe european academy of wind energy
Open Access WIND ENERGY SCIENCE DISCUSSIONS

2.3 Learning-based bias correction

Considering Eq. (1), the two BC contributions may become coupled, which complicates their individual identification. In particular, corrections introduced via $\boldsymbol{f}_0$ modify the generalized displacements and propagate to the measured outputs through $\delta\boldsymbol{q}$ in Eq. (1d), thereby influencing the estimation of $\boldsymbol{b}$.

To mitigate this coupling, $\boldsymbol{b}$ is first calibrated independently by neglecting $\boldsymbol{f}_0$. Once consistent estimates of $\boldsymbol{b}(\boldsymbol{s})$ are obtained across operating conditions $\boldsymbol{s}$, $\boldsymbol{b}$ is fixed and the dynamic correction term $\boldsymbol{f}_0$ is activated. As a simplified alternative, $\boldsymbol{b}$ may be omitted and only $\boldsymbol{f}_0$ retained, albeit at the cost of increased output error. An iterative alternation between both calibrations can further improve accuracy (Hoghooghi and Bottasso, 2026a).

The calibration procedure relies exclusively on measured outputs $\boldsymbol{y}$, since internal states and bias terms are not directly observable in practice. After calibration of $\boldsymbol{b}$, the identification of $\boldsymbol{f}_0$ proceeds in a structured multi-stage process to improve robustness, particularly for blade load estimation.

First, initial BC factors are estimated as linear functions of wind speed using a short representative dataset. This yields a baseline correction capturing dominant offsets and first-order wind-speed dependence.

Second, the obtained correction trends are systematically perturbed by vertical shifts while preserving slope, generating over- and under-corrected scenarios. This induces both positive and negative residuals across operating regimes, enriching the error space and improving the learning robustness of the subsequent model. Flapwise correction f_0^F is tuned prior to edgewise correction f_0^E, reflecting the dominant contribution of flapwise loads to blade bending and fatigue, particularly in Region II operation.

Third, a digital shadow is generated over a parametric sweep of BC factors and shifted correction profiles, producing a dataset that maps operating conditions and BC settings to resulting estimation errors. This enables systematic characterization of sensitivity to BC parameters.

Finally, a neural network is trained to learn the mapping between operating conditions, BC parameters, and load estimation errors. The training inputs consist of blade-root bending moment errors obtained from the parametric simulations, while the outputs correspond to the optimal correction terms f_0^F or f_0^E. During inference, the target error is enforced to a small value (e.g., 10^{-8}), enabling the network to identify BC parameters that minimize discrepancies between estimated and reference blade-root bending moments.

The input space includes wind speed V, rotor speed Ω, generator torque Q_{gen}, and either shear or harmonic descriptors. For the shear-based formulation, the input vector is defined as

$$\boldsymbol{i}_S = \{V, \alpha, k_h, \Omega, Q_{gen}\}^T, \tag{10}$$

where α and k_h denote vertical and horizontal shear parameters. Alternatively, the harmonic-based formulation is given by

$$\boldsymbol{i}_H = \{V, \boldsymbol{m}^T, \Omega, Q_{gen}\}^T, \tag{11}$$

where $\boldsymbol{m}$ contains blade-load harmonic components (cf. Eq. 9).

https://doi.org/10.5194/wes-2026-102
Preprint. Discussion started: 29 June 2026

eawe european academy of wind energy
Open Access WIND ENERGY SCIENCE DISCUSSIONS

The pitch angle may be included as an additional feature if it shows a significant correlation with bias evolution, particularly near the transition between Region II and Region III operation. Different input configurations and network architectures are therefore evaluated to identify the most suitable setup for each turbine application. The resulting model is integrated into the digital shadow workflow to provide data-driven bias correction for unseen operating conditions (Fig. 1).

3 Results

The digital shadow is evaluated using measurements from a 3.5 MW eno wind turbine (eno energy GmbH) under operational field conditions. The available signals include generator torque, rotor speed, pitch angle, tower-top fore-aft (FA) and side-side (SS) accelerations, blade-root flapwise and edgewise bending moments, as well as strain-gauge measurements of the tower-base bending moment components and blade bending moment at 25% span ($M_{B-25\%}$). All signals are sampled at 10 Hz. Following Sect. 2.1, the internal model of the filter is obtained by linearizing a proprietary encrypted Bladed model (DNV, 2023) over the full operating envelope from cut-in to cut-out.

3.1 Test site

The dataset was collected at a wind farm in northeast Germany near Kirch Mulsow (Rostock district, Mecklenburg-Vorpommern) during two measurement campaigns (17–30 October 2020). The raw measurements were used without calibration or post-processing, except for the removal of data gaps, turbine stops, faults, and non-power-production intervals.

The site, illustrated in Fig. 2, consists of open agricultural terrain with gentle orography and forested areas, located a few kilometers from the Baltic Sea. Four eno energy GmbH turbines (eno energy GmbH) are installed, and the digital shadow is applied to WT3. The corresponding turbine specifications are summarized in Table 2.

The measurement campaign is classified according to inflow conditions in Table 1. After preprocessing, approximately 49 h of clean free-stream operation was retained. Of these, 43 h (88%) are used for training, while 6 h are reserved for validation under representative steady conditions.

In addition, 23 h of complex inflow conditions were identified, including high shear and non-stationary atmospheric states. From this subset, 20 h (87%) are used for training and 3 h for validation.

Two further unseen validation datasets of 4.5 h and 3 h are included to assess generalization under mixed and transitional inflow regimes. These correspond to post-sunset and near-sunrise conditions characterized by intermittent atmospheric mixing and rapidly varying wind and shear. Excluding these periods from training provides a stringent test of model robustness.

Wind speed and shear estimators for this site were previously developed and validated in Schreiber et al. (2020); Bertelè et al. (2021).

3.2 Learning-based BC evaluation

The evaluation of the learning-based BC begins with the correction factors generated during training. Following Sect. 2.3, baseline BC factors are first identified as linear functions of wind speed using a short representative dataset, capturing the dominant

https://doi.org/10.5194/wes-2026-102
Preprint. Discussion started: 29 June 2026

eawe european academy of wind energy
Open Access WIND ENERGY SCIENCE DISCUSSIONS

Figure 2. Layout of the test site showing turbine positions. The digital shadow is evaluated on WT3. The red sector indicates the wind direction range during the measurement period, covering both simple and complex inflow conditions.

Table 1. Inflow conditions during the testing period.

Inflow conditions	Specific conditions	Time period	Total hours	Data split [hrs]
Simple inflow	Normal	17–31 Oct. 2020	49	43 (training) / 6 (testing)
Complex inflow	Extreme vertical shear	17–31 Oct. 2020	23	20 (training) / 3 (testing)
Mixed inflow	Post-sunset with intermittent mixing	18 Oct. 2020	4.5	4.5 (testing)
	Near-sunrise with strong fluctuating shear	31 Oct. 2020	3	3 (testing)

Table 2. Technical specifications of the WT3 turbine at the test site.

Wind turbine	Turbine specifications				
	Turbine model	Rotor diameter [m]	Hub height [m]	Rated power [MW]	Cut-in, rated, cut-out speeds [$\mathrm{m\,s^{-1}}$]
WT3	eno126	126	117	3.5	3.0, 12.5, 25.0

https://doi.org/10.5194/wes-2026-102
Preprint. Discussion started: 29 June 2026

eawe european academy of wind energy
Open Access WIND ENERGY SCIENCE DISCUSSIONS

220 bias trend across operating regions. These baseline curves are subsequently perturbed by vertical shifts while preserving slope, generating systematically over- and under-corrected cases. This construction expands the residual-error space and improves the identifiability of bias dynamics for the neural network. The resulting normalized flapwise and edgewise BC variations are shown in Fig. 3(a) and 3(b), respectively.

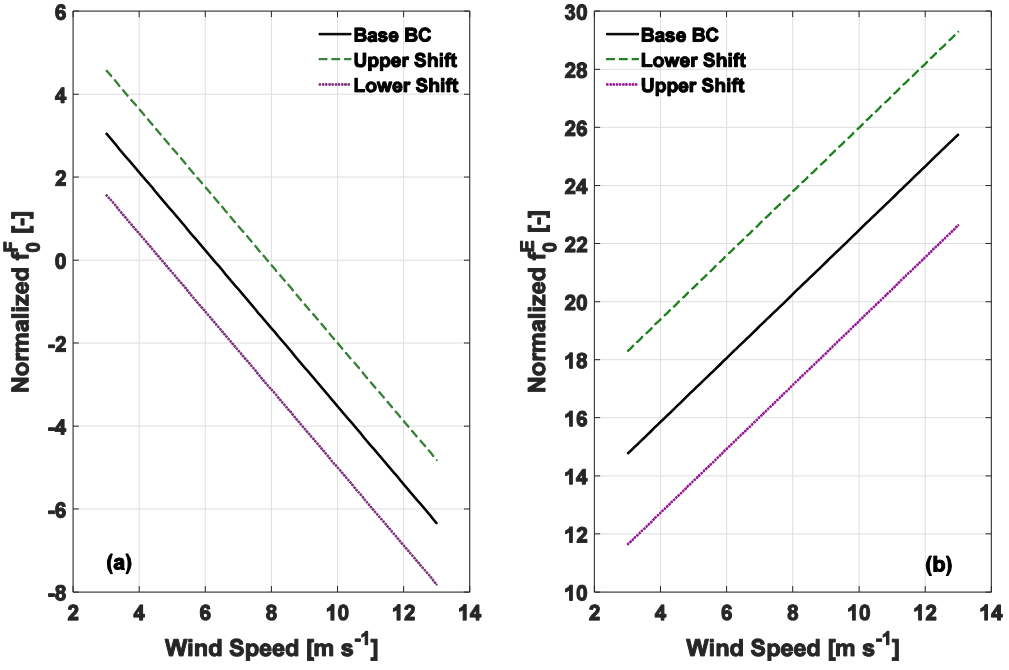

Figure 3. Normalized BC factor variations with wind speed for (a) flapwise and (b) edgewise directions, including baseline and shifted correction lines used for training. BC factors are shown in normalized form to preserve confidentiality while maintaining relative trends and slope consistency.

To illustrate the impact of BC settings on blade-root load estimation, a representative interval from 17 October 2020 (21:30–
225 23:00) is selected. This period exhibits sufficiently varied operating conditions while remaining quasi-stationary, enabling clear interpretation of BC effects. Figure 4 compares measured blade-root bending moments with estimates obtained using the baseline, upper-shift, and lower-shift BC configurations. The baseline corresponds to the initial linear BC estimate, while shifted cases represent systematic perturbations of identical slope. The results show that BC perturbations induce consistent over- and under-estimation across operating conditions, thereby generating both positive and negative residuals. This controlled
230 error diversification is essential for training, as it enables the neural network to learn the sensitivity of load-estimation errors to BC parameters, rather than relying on a single deterministic correction.

A feedforward deep neural network (DNN) is employed to learn the nonlinear mapping between operating conditions, BC parameters, and estimation errors. This formulation enables regression of optimal BC factors from observed error behavior.

https://doi.org/10.5194/wes-2026-102
Preprint. Discussion started: 29 June 2026

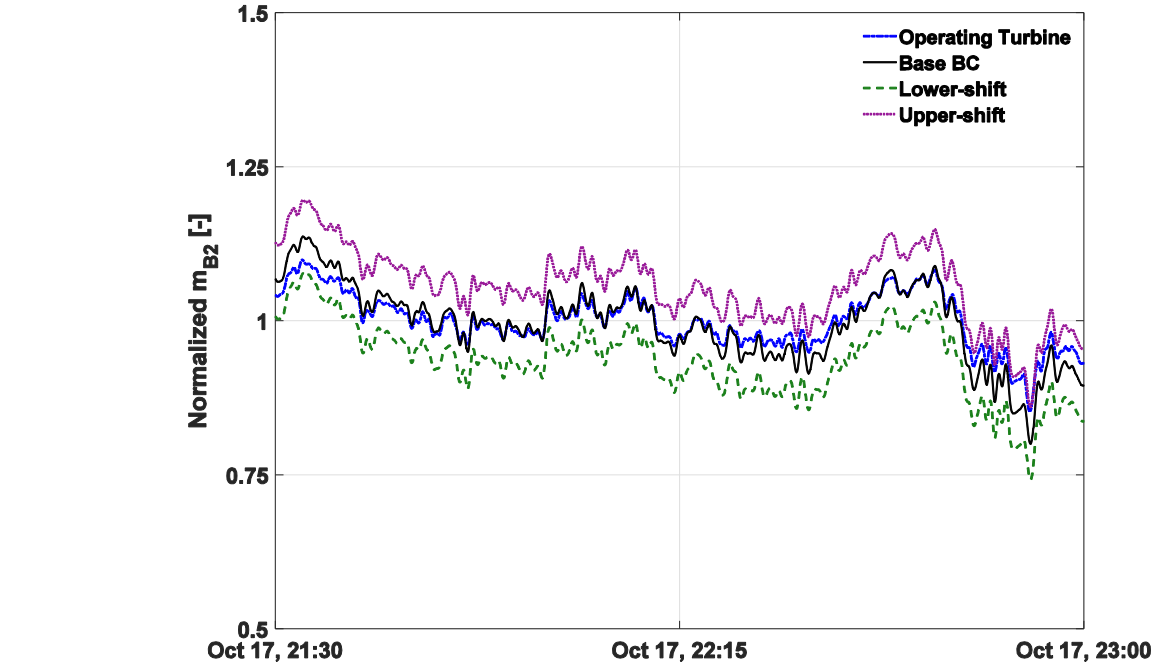

Figure 4. Comparison of blade-root bending moment estimates for 17 October 2020 (21:30–23:00) under different BC settings. The measured signal (blue dash-dot) is compared with baseline (black solid), lower-shift (green dashed), and upper-shift (purple dotted) corrections, illustrating the induced residual error structure used for training.

The model is trained in a supervised manner, with inputs consisting of operating conditions and simulation-derived estimation errors, and targets corresponding to optimal BC factors that minimize blade-root load discrepancies. Inputs include wind speed, rotor speed, generator torque, and either shear components or harmonic load features, depending on the configuration. Pitch angle is optionally incorporated when it exhibits a significant correlation with the estimation bias, particularly near the transition between Regions II and III and throughout Region III.

Rectified linear unit (ReLU) activation functions are used in all hidden layers due to their computational efficiency and stable gradient propagation (Nair and Hinton, 2010). The adaptive moment estimation (Adam) optimizer is used for parameter estimation, providing adaptive learning rates and robust convergence for nonlinear regression tasks (Kingma and Ba, 2015). Training is performed using mini-batch optimization with data shuffling at each epoch to reduce temporal correlation. To improve convergence stability, learning rate decay is applied in later epochs, and an exponential moving average (EMA) of network weights is maintained to reduce sensitivity to short-term fluctuations.

For simple inflow conditions, the optimal architecture is identified as 32–16–8–1, providing a balance between model complexity and generalization. Training is performed with a learning rate of 10^{-4} over 110 epochs. For complex inflow conditions, a larger architecture of 64–32–16–1 is required to capture increased variability due to shear and transient effects. The same

https://doi.org/10.5194/wes-2026-102
Preprint. Discussion started: 29 June 2026

eawe european academy of wind energy
Open Access WIND ENERGY SCIENCE DISCUSSIONS

training hyperparameters are used to ensure comparability. The training was performed on a standard desktop computer, taking approximately 1 hour, and constitutes a moderate computational effort limited to offline processing.

As explained previously in Sect. 2.3, two input formulations are evaluated: (i) shear-based inputs derived from observers (Sect. 2.2.2), and (ii) harmonic-based representations (Eq. 9). This avoids error propagation from secondary estimators and ensures a consistent comparison of BC performance. Wind speed, rotor speed, generator torque, and blade-root bending moment error are kept identical across configurations to ensure fair training conditions.

3.3 Simple inflow condition

Table 3 summarizes the root mean squared error (RMSE) and damage equivalent load (DEL) estimation errors for both normal and complex inflow conditions, as defined in Table 1. Figure 5(a) and 5(b) present the corresponding time histories of $M_{B-25\%}$ and M_{TB} for a representative day (26 Oct 2020) under normal inflow conditions, comparing measurements (blue dashed), the digital shadow without BC (red), and the learning-based BC digital shadow (yellow). All values are normalized to preserve turbine confidentiality.

For this representative case, the baseline without BC correction yields RMSE and DEL errors of 4% and 14%, respectively, for $M_{B-25\%}$. Incorporating a learning-based BC with shear-based input leads to a slight increase in RMSE to 6%, while reducing the DEL error to 8%. In contrast, the learning-based BC with harmonic-based input further improves performance, reducing the DEL error to 3% while maintaining an RMSE of 5%. As expected, the direct use of harmonic inputs reduces estimation errors by avoiding the additional uncertainty introduced by the neural network–based shear estimation. Overall, the learning-based BC approach provides accurate and robust DEL estimates for the quantities of interest.

Notably, for M_{TB}, the RMSE and DEL errors are reduced to 3% and 2%, respectively, when using corrected blade states obtained from the learning-based BC, demonstrating remarkably high accuracy for fatigue load analysis.

Table 3. Overview of RMSE and estimated output DEL errors for $M_{B-25\%}$ under different inflow conditions.

Inflow conditions	Time duration [hrs]	Estimation error $M_{B-25\%}$ [%]					
		No BC		Shear-based inputs		Harmonic-based inputs	
		RMSE	DELs	RMSE	DELs	RMSE	DELs
Simple inflow	6	4	14	6	8	5	3
Complex inflow	3	3	24	2	9	3	4

3.4 Complex inflow condition

Figure 6(a), 6(b), and 6(c) present the corresponding time histories of $M_{B-25\%}$, M_{TB}, and α, respectively, for a representative day (29 Oct 2020) under complex inflow conditions, comparing measurements (blue dashed), the digital shadow without BC (red), and the learning-based BC digital shadow (yellow).

https://doi.org/10.5194/wes-2026-102
Preprint. Discussion started: 29 June 2026

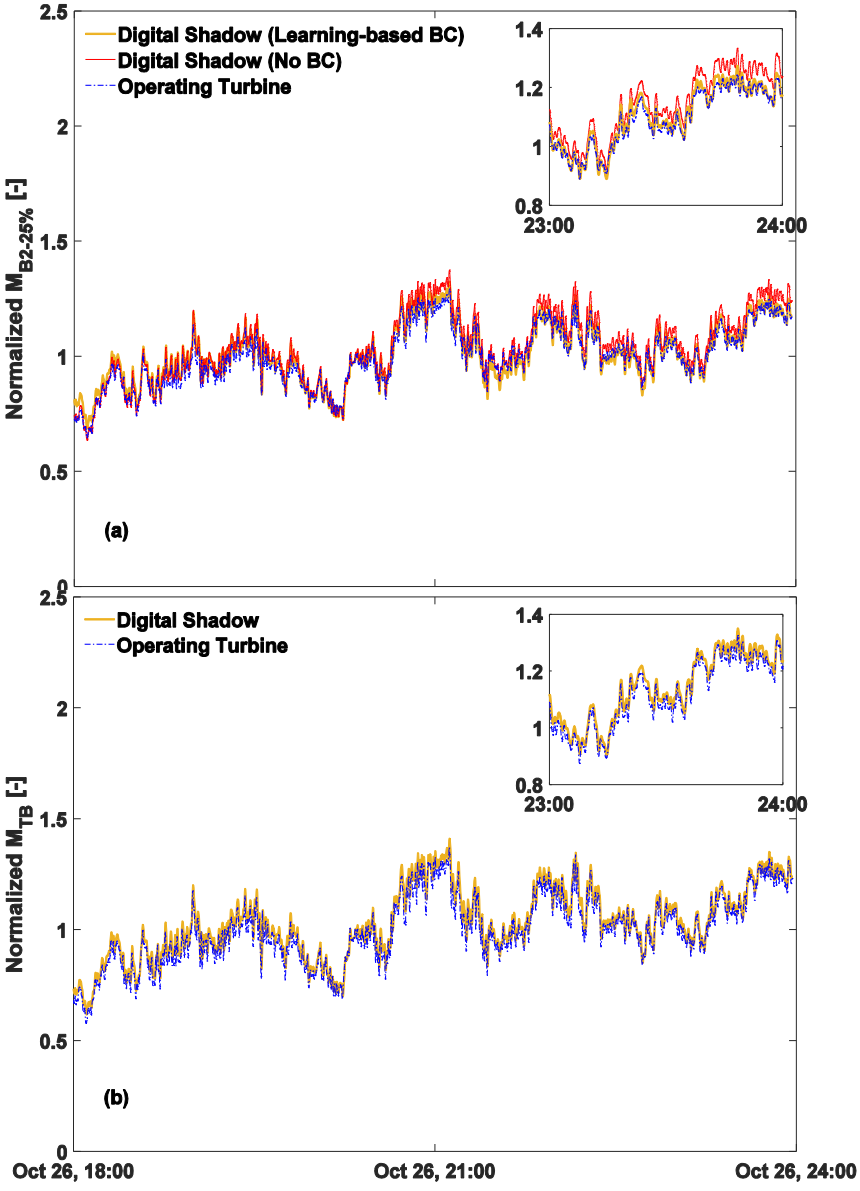

Figure 5. Time histories of the normalised $M_{B-25\%}$ **(a)** and M_{TB} **(b)** (26 Oct 2020, normal inflow). Measurements: dashed blue line; estimates of the digital shadow: solid red line; corrected estimates of the digital shadow using learning-based BC: solid yellow line.

https://doi.org/10.5194/wes-2026-102
Preprint. Discussion started: 29 June 2026

eawe european academy of wind energy
Open Access WIND ENERGY SCIENCE DISCUSSIONS

For this representative case, the baseline without BC correction yields RMSE and DEL errors of 3% and 24%, respectively, for $M_{B-25\%}$. Incorporating a learning-based BC with shear-based input reduces the RMSE and DEL error to 2% and 9%, respectively. In contrast, the learning-based BC with harmonic-based input further improves performance, reducing the DEL error to 4% while maintaining a similar RMSE. These results indicate the effectiveness of the learning-based BC approach for estimating the quantities of interest under high-shear, complex inflow conditions. Table 3 summarizes the corresponding error metrics. For M_{TB}, using learning-based BC-corrected blade states yields RMSE and DEL errors of 2% and 6%, respectively.

3.5 Mixed inflow condition

Two additional unseen validation datasets ($4.5\,\mathrm{h}$ and $3\,\mathrm{h}$, Table 1) are used to assess generalization under mixed and transitional inflow regimes, corresponding to post-sunset and near-sunrise conditions with intermittent mixing and rapidly varying wind and shear.

3.5.1 Post-sunset with intermittent mixing

Figure 7(a–d) presents the time series of $M_{B-25\%}$, M_{TB}, V, and α for a representative post-sunset day (18 Oct 2020) characterized by complex inflow conditions with intermittent mixing. During the initial period (green dashed box), wind speed increases rapidly and is accompanied by strong, highly variable vertical shear. The shear spans both the normal-to-high (< 0.3) and extreme (> 0.3) regimes (IEC, 2005; Hoghooghi and Bottasso, 2026b), exhibiting significant temporal fluctuations.

Accordingly, the performance of the digital shadow was evaluated using different trained DNNs. The baseline without BC correction yields RMSE and DEL errors of 4% and 15%, respectively, for $M_{B-25\%}$. Using a learning-based BC with harmonic input trained on simple inflow data reduces these to 3% and 5%. Training on complex inflow data yields comparable RMSE with a DEL error of 5%. A combined approach that switches between the two models based on vertical shear further improves performance to 3% RMSE and 4% DEL error. For M_{TB}, applying the bias-corrected blade states from the learning-based BC yields RMSE and DEL errors of 2% and 2%, respectively. Table 4 summarizes the corresponding error metrics.

These results highlight the effectiveness of a hybrid strategy under highly variable inflow conditions and suggest that separate models trained for low-, medium-, and high-wind-speed regimes could further improve performance across different turbine operating regions. Such a regime-wise decomposition enhances the local approximation accuracy of nonlinear bias characteristics.

3.5.2 Near-sunrise with strong fluctuating shear

Figure 8(a–e) presents the time histories of $M_{B-25\%}$, M_{TB}, V, α, and k_h for a representative near-sunrise period on 31 Oct 2020 under complex inflow conditions characterized by strongly fluctuating wind speed and shear. During the initial hours (green dashed box), the wind speed, together with both vertical and horizontal shear, increases rapidly, indicating highly unsteady inflow conditions.

https://doi.org/10.5194/wes-2026-102
Preprint. Discussion started: 29 June 2026

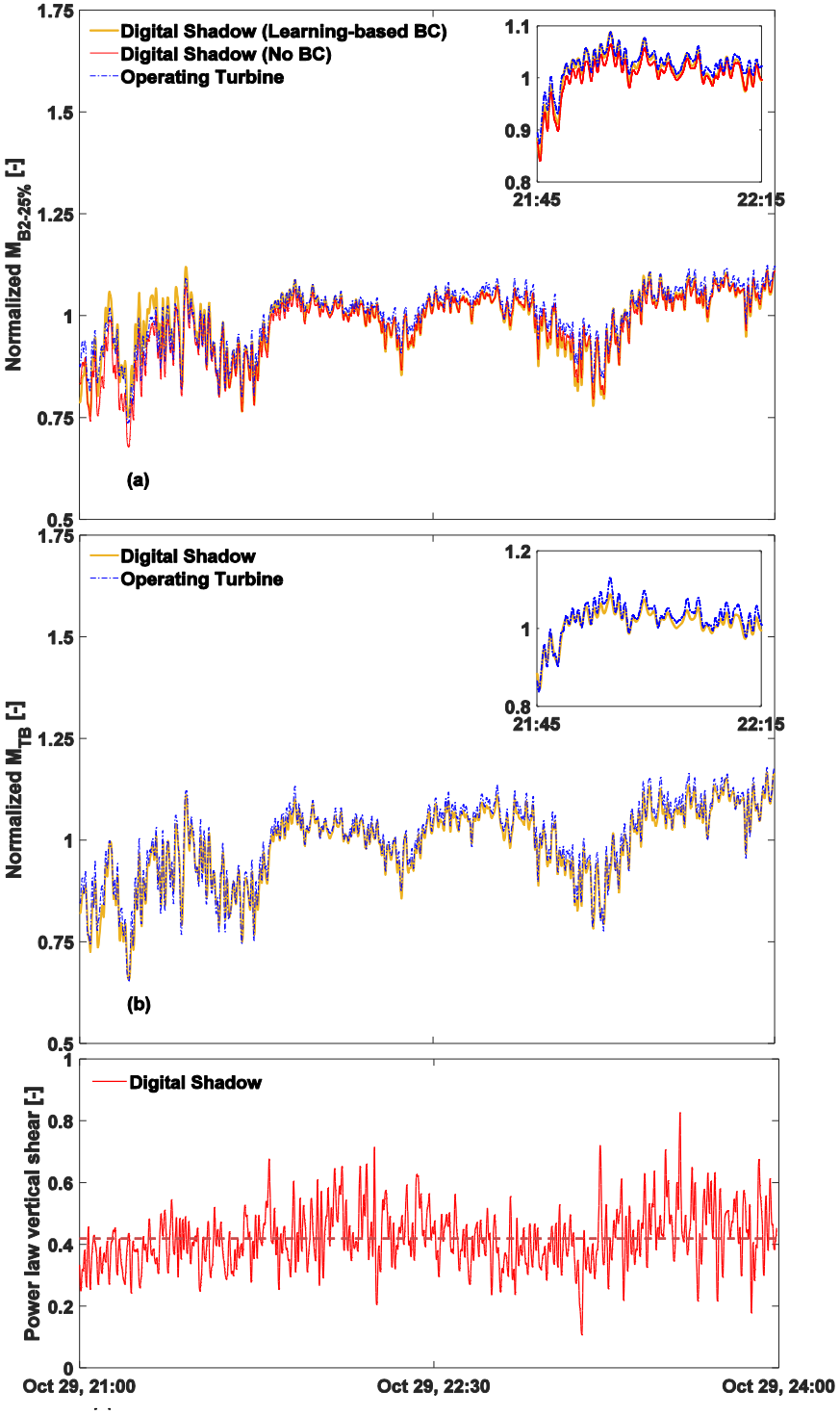

Figure 6. Time histories of the normalized $M_{B-25\%}$ **(a)**, M_{TB} **(b)**, and α (power-law vertical shear) **(b)** (29 Oct 2020, complex inflow). Measurements: dashed blue line; estimates of the digital shadow: solid red line; corrected estimates of the digital shadow using learning-based BC: solid yellow line.

https://doi.org/10.5194/wes-2026-102
Preprint. Discussion started: 29 June 2026

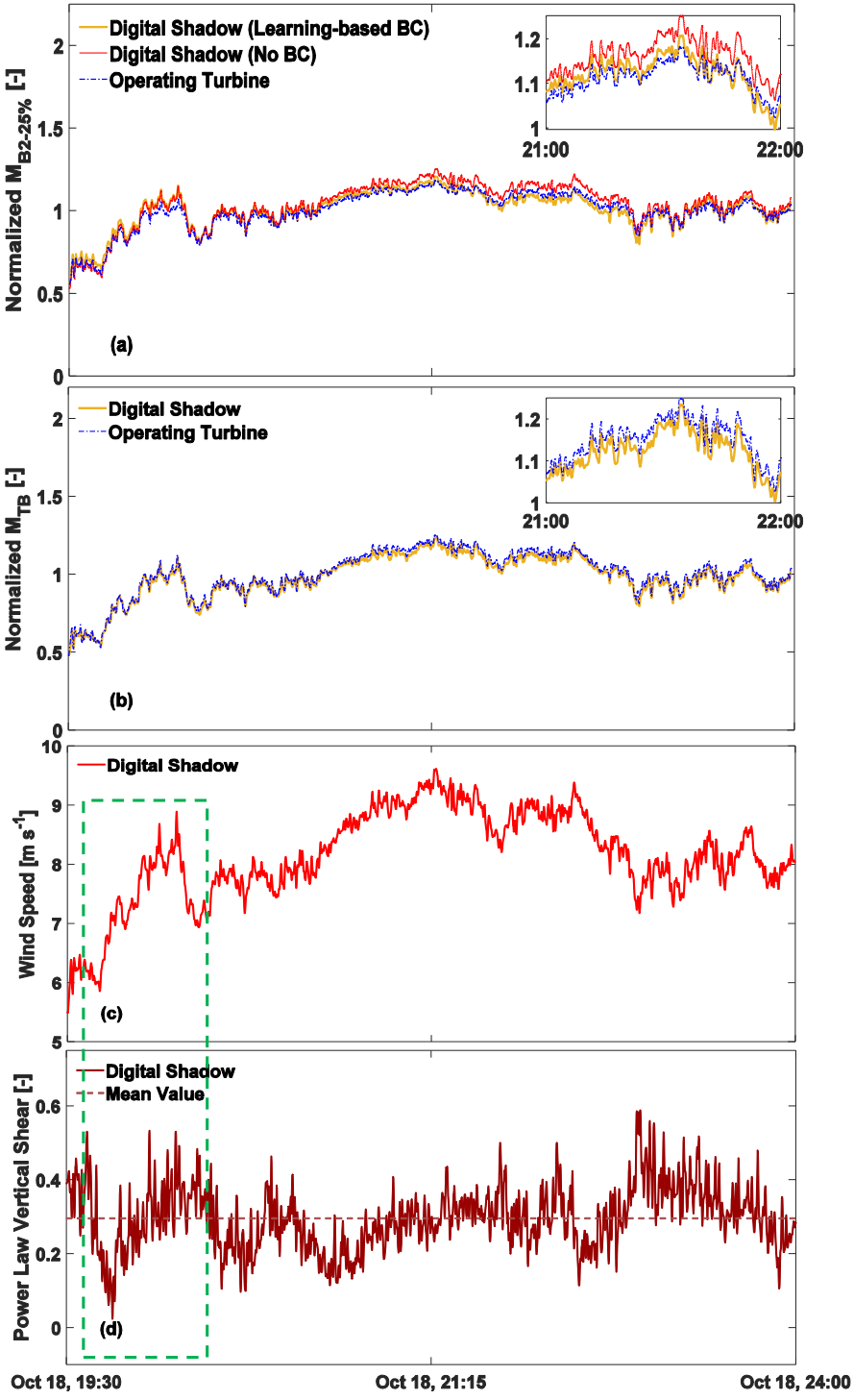

Figure 7. Time histories of normalized $M_{B-25\%}$ **(a)**, M_{TB} **(b)**, wind speed V **(c)**, and shear α **(d)** for 18 Oct 2020 under post-sunset mixed inflow conditions. Measurements are shown as dashed blue lines, baseline digital shadow estimates as solid red lines, and learning-based BC-corrected estimates as solid yellow lines.

https://doi.org/10.5194/wes-2026-102
Preprint. Discussion started: 29 June 2026

eawe european academy of wind energy
Open Access WIND ENERGY SCIENCE DISCUSSIONS

Table 4. Overview of RMSE and estimated output DEL errors for $M_{B\text{-}25\%}$ under mixed inflow conditions on 18 October 2020 during post-sunset periods with intermittent mixing.

Inflow conditions	Time duration [hrs]	Estimation error $M_{B-25\%}$ [%] using Harmonic-based inputs							
		No BC		DNN (simple inflow)		DNN (complex inflow)		Hybrid training	
		RMSE	DELs	RMSE	DELs	RMSE	DELs	RMSE	DELs
Mixed inflow (Post-sunset)	4.5	4	15	3	5	4	3	3	4

The baseline without BC correction yields RMSE and DEL errors of 7% and 6%, respectively, for $M_{B-25\%}$. Using a learning-based BC with harmonic input trained on simple inflow data reduces these to 5% and 5%. For M_{TB}, the use of corrected blade states results in RMSE and DEL errors of 3% and 8%, respectively.

Table 5. Overview of the RMSE and estimated output DEL errors for $M_{B\text{-}25\%}$ under mixed inflow conditions on 31 October 2020 during a near-sunrise period characterized by strongly fluctuating wind speed and shear.

Inflow conditions	Time duration [hrs]	Estimation error $M_{B-25\%}$ [%] using Harmonic-based inputs			
		No BC		DNN (simple inflow)	
		RMSE	DELs	RMSE	DELs
Mixed inflow (Near-sunrise)	3	7	6	5	5

4 Conclusions

A digital shadow framework for wind turbine load estimation has been developed by combining linearized aeroelastic modeling with a deep learning-based BC approach. This enables the use of encrypted industrial models (e.g., Bladed) while enhancing their predictive capability through data-driven corrections.

The proposed methodology employs a learning-based bias correction strategy that begins with initial linear fitting with respect to wind speed, followed by the generation of perturbed correction profiles to enrich the error space, and the construction of a digital shadow dataset through parametric simulations. Finally, a neural network is trained to map operating conditions and bias parameters to load estimation errors, enabling data-driven correction under unseen operating conditions.

The learning-based BC effectively compensates for model mismatch and limited inflow representation, significantly improving both absolute and fatigue load predictions. Across field data covering simple, complex, and mixed inflow conditions, blade bending moment DEL errors at the 25% span are reduced from 15%–25% to below 5%. These results demonstrate robust performance under highly variable atmospheric conditions and the ability to capture complex inflow–structure interactions.

https://doi.org/10.5194/wes-2026-102
Preprint. Discussion started: 29 June 2026

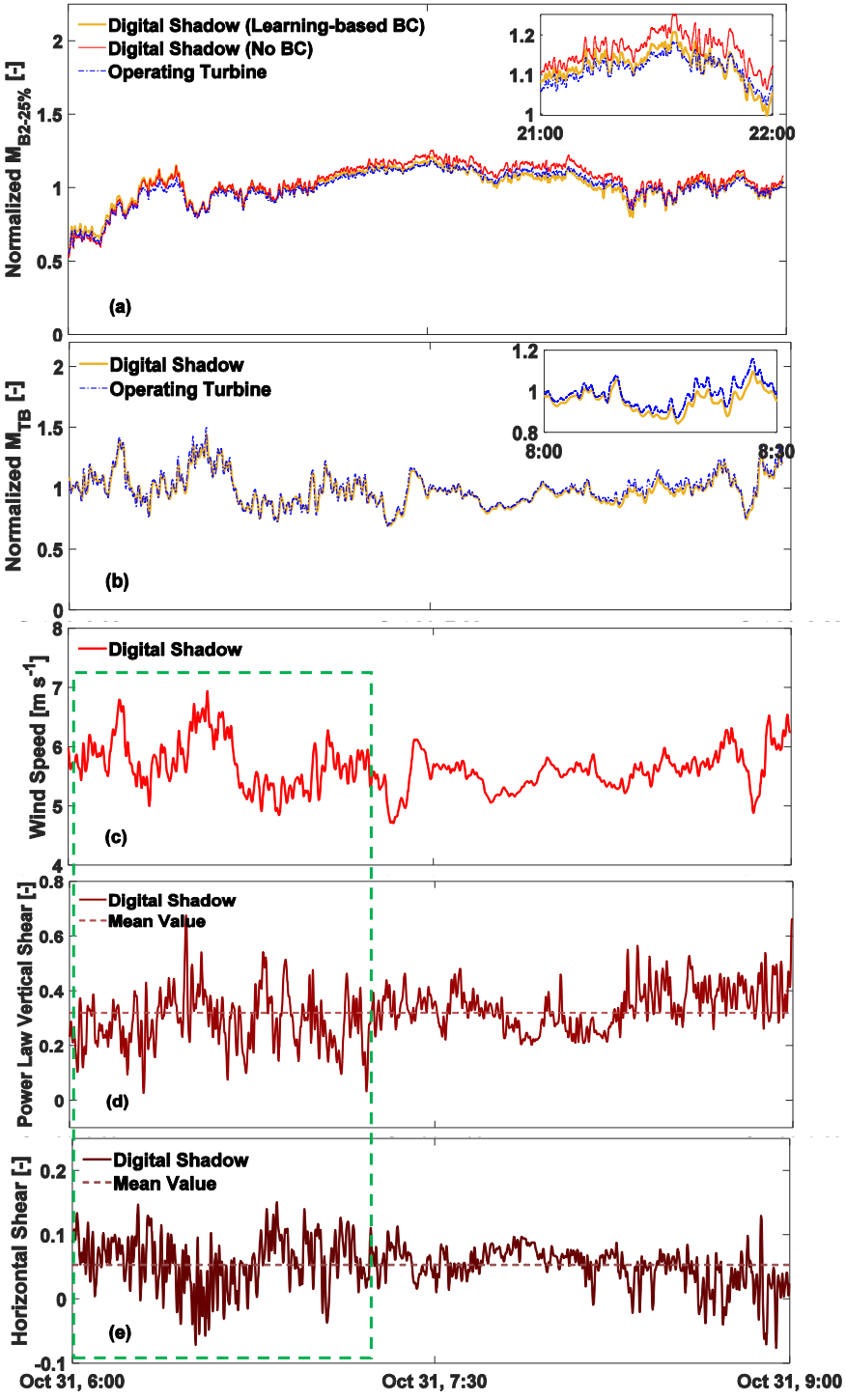

Figure 8. Time histories of normalized $M_{B\text{-}25\%}$ **(a)**, M_{TB} **(b)**, wind speed V **(c)**, vertical shear α **(d)**, and horizontal shear k_h **(e)** on 31 Oct 2020 during near-sunrise mixed inflow conditions. Measurements are shown as dashed blue lines, baseline digital shadow estimates as solid red lines, and learning-based BC-corrected estimates as solid yellow lines.

https://doi.org/10.5194/wes-2026-102
Preprint. Discussion started: 29 June 2026

eawe european academy of wind energy
Open Access WIND ENERGY SCIENCE DISCUSSIONS

The overall error levels are remarkably lower than those reported in previous studies, typically in the range of 10%–15% (Branlard et al., 2020a, b, 2024), while also accounting for additional degrees of freedom and blade dynamics, thereby underscoring the effectiveness of the proposed method.

Future work will extend the framework to more challenging scenarios, including waked, yawed, and offshore inflow conditions, as well as different turbine types, to further assess its robustness and generalization capability. Moreover, the methodology will be validated under extreme and transient operating conditions—such as gust events, curtailment, and shutdown/start-up sequences—to improve load observability and enhance prediction accuracy.

Looking ahead, the proposed approach provides a direct pathway toward a digital twin by integrating real-time SCADA and sensor data for continuous model adaptation. This would enable not only accurate load estimation but also predictive maintenance, operational optimization, and scenario analysis. In particular, the ability to anticipate fatigue-critical conditions and adjust control strategies highlights the potential of this framework as a scalable foundation for next-generation wind turbine digital twins.

https://doi.org/10.5194/wes-2026-102
Preprint. Discussion started: 29 June 2026

eawe european academy of wind energy
Open Access WIND ENERGY SCIENCE DISCUSSIONS

Appendix A: Nomenclature

$\boldsymbol{b}$	Vector of sensor biases
$\boldsymbol{f}_0$	Static correction force
$\boldsymbol{i}$	Input vector of the inflow estimator
$\boldsymbol{p}$	Vector of free network parameters
$\boldsymbol{q}$	Vector of generalized displacements
$\boldsymbol{s}$	Vector of scheduling parameters
$\boldsymbol{u}$	Input vector
$\boldsymbol{v}$	Vector of generalized velocities
$\boldsymbol{y}$	Vector of outputs for Kalman innovation
$\boldsymbol{z}$	Vector of other outputs of interest
$\boldsymbol{\nu}$	Measurement noise vector
$\boldsymbol{\omega}$	Process noise vector
A	Rotor swept area
c	Generic output of the wind inflow characteristic observer
C_p	Power coefficient
d	Displacement
J	Rotor inertia
κ_h	Horizontal shear
M	Bending moment resultant
m	Bending moment component
Q	Torque
R	Rotor radius
V	Wind speed
α	Vertical power-law shear exponent
γ	Misalignment angle
$\boldsymbol{\epsilon}$	Output correction term
θ	Blade pitch angle
λ	Tip speed ratio
ρ	Air density
ψ	Rotor azimuthal position

https://doi.org/10.5194/wes-2026-102
Preprint. Discussion started: 29 June 2026

eawe european academy of wind energy
Open Access WIND ENERGY SCIENCE DISCUSSIONS

	Ω	Rotor rotational speed
	$(\cdot)^{E}$	Edgewise component
	$(\cdot)^{F}$	Flapwise component
	$(\cdot)^{FA}$	Fore-aft component
	$(\cdot)^{SS}$	Side-side component
	$(\cdot)^{IP}$	In-plane component
	$(\cdot)^{OP}$	Out-of-plane component
	$(\cdot)^{NN}$	Quantity corrected by a neural network
	$(\cdot)_{1c}$	1P cosine component
	$(\cdot)_{1s}$	1P sine component
	$(\cdot)_{Bi}$	Quantity referred to the ith blade
	$(\cdot)_{B-s\%}$	Quantity referred to the $s\%$ spanwise location
	$(\cdot)_{TB}$	Quantity referred to the base of the tower
	$(\cdot)_{E}$	Estimated quantity
	$(\cdot)_{M}$	Measured quantity
	$(\cdot)_{0}$	Reference equilibrium condition
	$\delta(\cdot)$	Perturbation about a reference equilibrium condition
	Adam	Adaptive moment estimation
	BC	Bias correction
	DEL	Damage-equivalent load
	DNN	Deep neural network
	DOF	Degree of freedom
	EMA	Exponential moving average
	FA	Fore-aft
	FEM	Finite element method
	LUT	Look-up table
	NN	Neural network
	OEM	Original equipment manufacturer
	ReLU	Rectified linear unit
	RMSE	Root mean squared error
	ROM	Reduced order model
	SCADA	Supervisory control and data acquisition

https://doi.org/10.5194/wes-2026-102
Preprint. Discussion started: 29 June 2026

SS	Side-side
WT	Wind turbine

Data availability. All figures and the data used to generate them can be retrieved in Pickle Python and MATLAB formats via https://doi.org/10.5281/zenodo.20051734. The field dataset is the property of eno energy systems GmbH.

Author contributions. HH developed the new BC training methodology, implemented the digital shadow, performed the numerical simulations, and processed the field dataset. CLB developed the core digital shadow concept and supervised the work. Both authors contributed equally to the interpretation of the results and to the writing of the paper.

Competing interests. At least one of the (co-)authors is a member of the editorial board of *Wind Energy Science*.

Acknowledgements. The technical assistance from Marta Bertelè and Carlo R. Sucameli is acknowledged and greatly appreciated. The authors express their gratitude to eno energy systems GmbH, which granted access to the turbine aeroelastic model and to the field dataset.

Financial support. This work has been supported in part by the PowerTracker (FKZ: 03EE2036A), CompactWind II project (FKZ: 0325492G), and Life-Odometer (FKZ: 03EE3037B) projects, which receive funding from the German Federal Ministry for Economic Affairs and Climate Action (BMWK). Additional support has been provided by the MERIDIONAL project, which receives funding from the European Union's Horizon Europe program under the grant agreement no. 101084216.

https://doi.org/10.5194/wes-2026-102
Preprint. Discussion started: 29 June 2026

eawe european academy of wind energy
Open Access WIND ENERGY SCIENCE DISCUSSIONS

References

Abdallah, I., Tatsis, K., and Chatzi, E.: Fatigue assessment of a wind turbine blade when output from multiple aero-elastic simulators are available, Procedia Engineering, 199, 3170–3175, https://doi.org/https://doi.org/10.1016/j.proeng.2017.09.509, x International Conference on Structural Dynamics, EURODYN 2017, 2017.

Anand, A. and Bottasso, C. L.: Reducing Plant-Model Mismatch for Economic Model Predictive Control of Wind Turbine Fatigue by a Data-Driven Approach, in: 2023 American Control Conference (ACC), 979-8-3503-2806-6, pp. 1473–1479, https://doi.org/10.23919/ACC55779.2023.10156501, 2023.

Bertelè, M., Bottasso, C. L., and Schreiber, J.: Wind inflow observation from load harmonics: initial steps towards a field validation, Wind Energ. Sci., 6, 759–775, https://doi.org/10.5194/wes-6-759-2021, 2021.

Bertelè, M., Meyer, P. J., Sucameli, C. R., Fricke, J., Wegner, A., Gottschall, J., and Bottasso, C. L.: The rotor as a sensor – Observing shear and veer from the operational data of a large wind turbine, Wind Energ. Sci., 9, 1419–1429, https://doi.org/10.5194/wes-9-1419-2024, 2024.

Bottasso, C., Cacciola, S., and Schreiber, J.: Local wind speed estimation, with application to wake impingement detection, Renewable Energy, 116, 155–168, https://doi.org/https://doi.org/10.1016/j.renene.2017.09.044, 2018.

Branlard, E., Giardina, D., and Brown, C. S. D.: Augmented Kalman filter with a reduced mechanical model to estimate tower loads on a land-based wind turbine: a step towards digital-twin simulations, Wind Energ. Sci., 5, 1155–1167, https://doi.org/10.5194/wes-5-1155-2020, 2020a.

Branlard, E., Jonkman, J., Dana, S., and Doubrawa, P.: A digital twin based on OpenFAST linearizations for real-time load and fatigue estimation of land-based turbines, J. Phys.: Conf. Ser., 1618, 022 030, https://doi.org/10.1088/1742-6596/1618/2/022030, 2020b.

Branlard, E., Jonkman, J., Brown, C., and Zhang, J.: A digital twin solution for floating offshore wind turbines validated using a full-scale prototype, Wind Energ. Sci., 9, 1–24, https://doi.org/10.5194/wes-9-1-2024, 2024.

Branlard, E. S. P.: Flexible multibody dynamics using joint coordinates and the Rayleigh-Ritz approximation: The general framework behind and beyond Flex, Wind Energy, 22, 877–893, https://doi.org/https://doi.org/10.1002/we.2327, 2019.

Dimitrov, N., Kelly, M. C., Vignaroli, A., and Berg, J.: From wind to loads: wind turbine site-specific load estimation with surrogate models trained on high-fidelity load databases, Wind Energ. Sci., 3, 767–790, https://doi.org/10.5194/wes-3-767-2018, 2018.

DNV: Bladed, https://www.dnv.com, version 4.11, 2023.

eno energy GmbH: Eno energy GmbH, last access on 15.02.2024.

Evans, M., Han, T., and Shuchun, Z.: Development and validation of real time load estimator on Goldwind 6 MW wind turbine, J. Phys.: Conf. Ser., 1037, 032 021, https://doi.org/10.1088/1742-6596/1037/3/032021, 2018.

Grewal, M. S. and Andrews, A. P.: Kalman Filtering: Theory and Practice with MATLAB, John Wiley & Sons, Inc., 2008.

Grewal, M. S. and Andrews, A. P.: Kalman Filtering: Theory and Practice Using Matlab, John Wiley & Sons, Inc., https://doi.org/https://doi.org/10.1002/9781118984987, 2014.

Guilloré, A., Campagnolo, F., and Bottasso, C. L.: A control-oriented load surrogate model based on sector-averaged inflow quantities: capturing damage for unwaked, waked, wake-steering and curtailed wind turbines, J. Phys.: Conf. Ser., 2767, 032 019, https://doi.org/10.1088/1742-6596/2767/3/032019, 2024.

Hochreiter, S. and Schmidhuber, J.: Long Short-Term Memory, Neural Computation, 9, 1735–1780, 1997.

https://doi.org/10.5194/wes-2026-102
Preprint. Discussion started: 29 June 2026

Hoghooghi, H. and Bottasso, C. L.: Digital shadows with optimized bias correction for accurate wind turbine fatigue load estimation, Journal of Physics: Conference Series, 3224, 062 003, https://doi.org/10.1088/1742-6596/3224/6/062003, 2026a.

Hoghooghi, H. and Bottasso, C. L.: A wind turbine digital shadow for complex inflow conditions, Wind Energy Science, 11, 373–393, https://doi.org/10.5194/wes-11-373-2026, 2026b.

Hoghooghi, H., Chokani, N., and Abhari, R.: Effectiveness of individual pitch control on a 5MW downwind turbine, Renewable Energy, 139, 435–446, https://doi.org/https://doi.org/10.1016/j.renene.2019.02.088, 2019.

Hoghooghi, H., Chokani, N., and Abhari, R. S.: Individual Blade Pitch Control for Extended Fatigue Lifetime of Multi-Megawatt Wind Turbines, J. Phys.: Conf. Ser., 1618, 022 008, https://doi.org/10.1088/1742-6596/1618/2/022008, 2020.

Hoghooghi, H., Bertelè, M., Anand, A., and Bottasso, C. L.: A wind turbine digital shadow with tower and blade degrees of freedom - Preliminary results and comparison with a simple tower fore-aft model, J. Phys.: Conf. Ser., 2767, 032 026, https://doi.org/10.1088/1742-6596/2767/3/032026, 2024.

IEC: IEC 61400-1 Wind turbines: Design requirements, International Electrotechnical Commision, 2005.

Iliopoulos, A., Shirzadeh, R., Weijtjens, W., Guillaume, P., Hemelrijck, D. V., and Devriendt, C.: A modal decomposition and expansion approach for prediction of dynamic responses on a monopile offshore wind turbine using a limited number of vibration sensors, Mech. Syst. Signal Process., 68-69, 84–104, https://doi.org/https://doi.org/10.1016/j.ymssp.2015.07.016, 2016.

Jacquelin, E., Bennani, A., and Hamelin, P.: Force reconstruction: analysis and regularization of a deconvolution problem, J. Sound Vib., 265, 81–107, https://doi.org/https://doi.org/10.1016/S0022-460X(02)01441-4, 2003.

Juang, J.-N. and Pappa, R. S.: The eigensystem realization algorithm and its application to modal parameter identification, Journal of Sound and Vibration, 3, 221–235, 1985.

Kim, K.-H., Bertelè, M., and Bottasso, C. L.: Wind inflow observation from load harmonics via neural networks: A simulation and field study, Renewable Energy, 204, 300–312, https://doi.org/https://doi.org/10.1016/j.renene.2022.12.051, 2023.

Kingma, D. P. and Ba, J. L.: Adam: A Method for Stochastic Optimization, International Conference on Learning Representations (ICLR), arXiv preprint arXiv:1412.6980, 2015.

Lea, C. e. a.: Temporal Convolutional Networks for Action Segmentation and Detection, in: CVPR, 2017.

Ljung, L.: System Identification: Theory for the User, Prentice-Hall, 1999.

Mendez Reyes, H., Kanev, S., Doekemeijer, B., and van Wingerden, J.-W.: Validation of a lookup-table approach to modeling turbine fatigue loads in wind farms under active wake control, Wind Energ. Sci., 4, 549–561, https://doi.org/10.5194/wes-4-549-2019, 2019.

Nair, V. and Hinton, G. E.: Rectified Linear Units Improve Restricted Boltzmann Machines, Proceedings of the 27th International Conference on Machine Learning (ICML), pp. 807–814, 2010.

Noppe, N., Iliopoulos, A., Weijtjens, W., and Devriendt, C.: Full load estimation of an offshore wind turbine based on SCADA and accelerometer data, J. Phys.: Conf. Ser., 753, 072 025, https://doi.org/10.1088/1742-6596/753/7/072025, 2016.

Olatunji, O. O., Adedeji, P. A., Madushele, N., and Jen, T.-C.: Overview of Digital Twin Technology in Wind Turbine Fault Diagnosis and Condition Monitoring, in: IEEE 12th ICMIMT, pp. 201–207, https://doi.org/10.1109/ICMIMT52186.2021.9476186, 2021.

Schreiber, J., Bottasso, C. L., and Bertelè, M.: Field testing of a local wind inflow estimator and wake detector, Wind Energ. Sci., 5, 867–884, https://doi.org/10.5194/wes-5-867-2020, 2020.

Schröder, L., Dimitrov, N. K., Verelst, D. R., and Sørensen, J. A.: Wind turbine site-specific load estimation using artificial neural networks calibrated by means of high-fidelity load simulations, J. Phys.: Conf. Ser., 1037, 062 027, https://doi.org/10.1088/1742-6596/1037/6/062027, 2018.

https://doi.org/10.5194/wes-2026-102
Preprint. Discussion started: 29 June 2026

Soltani, M. N., Knudsen, T., Svenstrup, M., Wisniewski, R., Brath, P., Ortega, R., and Johnson, K.: Estimation of rotor effective wind speed: A comparison, IEEE Transactions on Control Systems Technology, 21, 1155 – 1167, https://doi.org/10.1109/TCST.2013.2260751, 2013.

Song, Z., Hackl, C. M., Anand, A., Thommessen, A., Petzschmann, J., Kamel, O., Braunbehrens, R., Kaifel, A., Roos, C., and Hauptmann, S.: Digital Twins for the Future Power System: An Overview and a Future Perspective, Sustainability, 15, 2023.

Van Overschee, P. and De Moor, B.: Subspace Identification for Linear Systems: Theory—Implementation—Applications, Springer, 1996.

Vettori, S., Di Lorenzo, E., Peeters, B., and Chatzi, E.: A virtual sensing approach to operational modal analysis for wind turbine blades, 2020.

Ziegler, L., Smolka, U., Cosack, N., and Muskulus, M.: Brief communication: Structural monitoring for lifetime extension of offshore wind monopiles: can strain measurements at one level tell us everything?, Wind Energ. Sci., 2, 469–476, https://doi.org/10.5194/wes-2-469-2017, 2017.